JOURNAL OF MATERIALS SCIENCE 27 (1992) 4421–4428

# Mechanical behaviour and failure phenomenon of an *in situ* toughened silicon nitride

J. A. SALEM, S. R. CHOI, M. R. FREEDMAN
*NASA Lewis Research Center, Cleveland, OH, USA*
M. G. JENKINS
*Oak Ridge National Laboratory, Oak Ridge, TN, USA*

The Weibull modulus, fracture toughness and crack-growth resistance of an *in situ* toughened, silicon nitride material used to manufacture a turbine combustor were determined from room temperature to 1371 °C. The material exhibited an elongated grain structure that resulted in improved fracture toughness, non-linear crack-growth resistance, and good elevated-temperature strength. However, low-temperature strength was limited by grains of excessive length (30–100 μm). These excessively long grains were surrounded by regions rich in sintering additives.

## 1. Introduction

The need for more fuel-efficient transportation and lower engine emissions has made ceramics increasingly important materials for structural components of engines. Although the high-temperature strength of ceramics has been advantageous, the low fracture toughness and poor reliability has been an impediment. Many methods of toughening ceramics have been attempted; however, the simplest method has been microstructural texturing or *in situ* toughening.

The mechanical properties of components made from *in situ* toughened ceramics are controlled by the processing methods used in production. Thus, reliability analysis and life prediction of such ceramic structural components requires design data determined directly from components or access to relatively large experimental data bases. Presently, data bases for such materials are limited. The objective of this work was to determine the mechanical properties and failure behaviour of an *in situ* toughened, silicon nitride material processed in the form of a turbine combustor. The mechanical properties were subsequently used for reliability analysis [1, 2].

## 2. Experimental procedure

### 2.1. Material

A mixture of silicon nitride powder ($Si_3N_4$), sintering aids and a polymeric binder were milled in a polyethylene jar with $Si_3N_4$ media for 3 days. The resulting slurry was separated from the media, dried and granulated. The granulated powder was cold isostatically pressed at 100 MPa to form a cylindrical combustor. The combustor was green machined to near final shape, dewaxed and then sintered in a nitrogen atmosphere. Final machining produced the combustor shown in Fig. 1. Typical microstructure is exhibited in Fig. 2. The grain structure was delineated with a modified plasma etching procedure [3]. No anisotropy was observed in metallographic sections of transverse and longitudinal orientations.

### 2.2. Mechanical testing

Young's modulus and Poisson's ratio between room temperature and 1400 °C were determined by sonic resonance in accordance with ASTM method C848-76 [4]. Young's modulus was also determined at room temperature by strain gauging a four-point bend specimen.

Test specimens for strength and fracture toughness measurements were machined from the combustor and heat treated in air at 1150 °C for 1.5 h to relieve residual stress and heal machining damage. Four-point bend strength was determined at temperatures of 25, 1000, and 1371 °C at a displacement rate of 0.5 mm $min^{-1}$. The strength specimens measured 3 mm × 4 mm in height and width, and the inner and outer spans of the flexure fixture were 10 and 30 mm, respectively.

Fracture toughness was determined with the single-edged precracked beam (SEPB) [5], single-edged notched beam (SENB) and chevron notch [6] methods in three-point bending. Specimens measured 3 mm × 4 mm × 30 mm in width, height and span, and the notch width of the SENB specimen was 0.050 mm. The chevron-notch parameters, $\alpha_0$ and $\alpha_1$, were 0.625 and 1.0, respectively. The stress intensity factor coefficient was determined with a slice model [6] and an interlaminar shear factor of 1.453. The SEPB specimens were tested at a displacement rate of 0.5 mm $min^{-1}$, and chevron-notch specimens were tested at 0.005 mm $min^{-1}$. The low displacement rate used for chevron-notch testing was required to ensure stable crack extension. Such slow rates were successful in the testing of $SiC/TiB_2$ composites [7].

0022–2461 

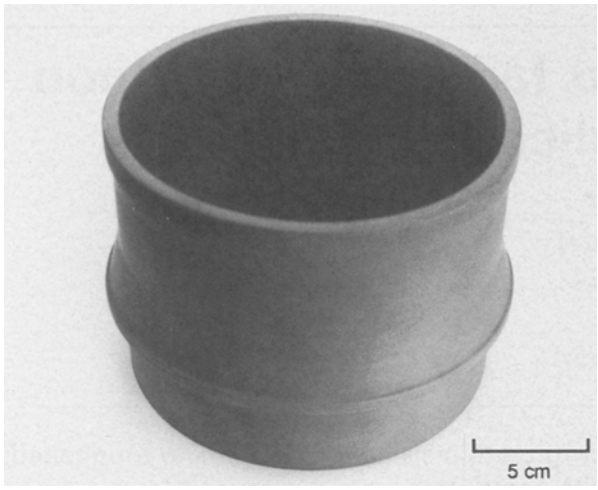


*Figure 1* View of the silicon nitride combustor.

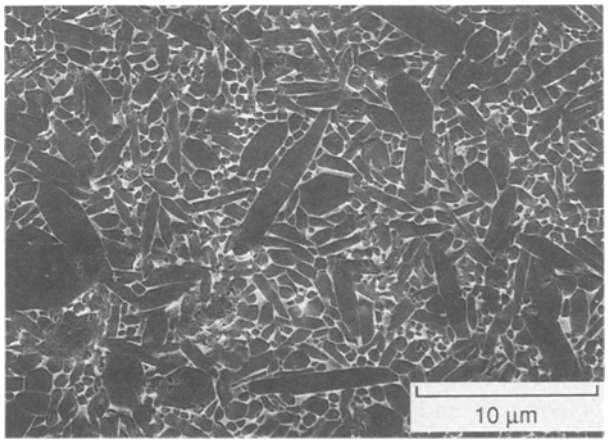


*Figure 2* Plasma-etched microstructure of *in situ* toughened silicon nitride.

Room-temperature *R*-curve behaviour was estimated using the indentation strength technique proposed by Krause [8]. The test specimens were 3 mm × 5.6 mm × 25 mm modulus of rupture (MOR) bars. The centre of the tensile surface was polished and indented with a Vickers microhardness indentor at loads ranging from 49–196 N. The subsequent strength tests of the indented samples were conducted using a four-point bend fixture with 9.5 and 20 mm spans and a displacement rate of 0.2 mm $min^{-1}$ in room-temperature air. Three specimens were tested at each indentation load.

## 3. Results and discussion

### 3.1. Young's modulus and Poisson's ratio

Young's modulus exhibited a continuous drop from 309 GPa at 25 °C to 281 GPa at 1371 °C, indicating a slight sensitivity to temperature. The Young's modulus determined from strain gauge readings at 25 °C was 299 MPa, about 3% lower than the sonically determined value. Poisson's ratio varied about an average of 0.27 ± 0.04 between room temperature and 1400 °C.

### 3.2. Strength

Weibull parameters can be determined by the uncensored or the censored data technique [9, 10]. For uncensored data the parameters are determined from

$$\ln\ln\left(\frac{1}{1-F}\right) = m_r \ln\left(\frac{\sigma_f}{\sigma_r}\right) \quad (1)$$

where $\sigma_f$ is the fracture strength, $\sigma_r$ is the characteristic strength, $m_r$ is the Weibull modulus and $F$ is the cumulative failure probability based on

$$F = \frac{j - 0.3}{J + 0.4} \quad (2)$$

where $J$ is the total number of specimens, and $j$ is the specimen rank as assigned by ordering specimens from weakest to strongest. It should be noted that the characteristic strength is dependent on specimen volume and should not be confused with the scale parameter which is independent of volume.

For censored data, the specimens are also ordered from weakest to strongest, however, the parameters are determined by adding an extra increment of rank to account for the presence of two flaw populations. The extra increment of rank is given by

$$\Delta = \frac{(J + 1) - j_i}{1 + J_0} \quad (3)$$

where $j_i$ is the previous ranking and $J_0$ is the number of samples beyond the present censored set. The adjusted ranking is determined by adding the increment determined from Equation 3 to the previous ranking. The associated failure probability and censored Weibull parameters are determined from Equations 1 and 2 and the adjusted rank.

Failures were censored by location of the origin (surface connected flaws versus volume flaws), regardless of their processing source or nature (e.g. grain, pore, or surface damage). Flaw location as well as its nature were determined with optical microscopy or scanning electron microscopy (SEM) as necessary.

Summaries of bend-strength test results for both uncensored and censored data are given in Tables I and II, respectively. Strength decreased from an average, $\bar{\sigma}_f$, of 671 ± 41 MPa at room temperature to 520 ± 54 MPa at 1371 °C, with a corresponding decrease of Weibull modulus from 18.90 to 11.25 (Table I). All observed failure origins were either large, 30–100 μm grains with hexagonal cross-sections, or 15–70 μm diameter pores. The coarse grains were frequently connected to glassy regions. These regions were analysed with energy dispersive analysis and determined to be rich in sintering additives. Failure origins of different natures and locations are shown in Fig. 3, and a glassy region attached to a coarse grain is shown in Fig. 4.

The population of volume type failures observed at 25 and 1000 °C was insufficient for accurate statistical characterization; however, at 1371 °C, nearly 50% of the specimens failed from volume flaws. This increase in incidence of volume failures with increasing test temperature may indicate a further healing of surface-connected flaws during heating of the specimens to

TABLE I Average strength, uncensored Weibull parameters (LS), and nature of failure origins

| Temperature (°C) | $\bar{\sigma}_f$ [a] (MPa) | $\sigma_r$ (MPa) | Weibull modulus | Flaw location | Flaw type | Number of occurrences |
|---|---|---|---|---|---|---|
| 25 | 671 (41) | 690 | 18.90 | Surface | Grain | 14 |
| | | | | Surface | Pore | 6 |
| | | | | Surface | ND[b] | 6 |
| | | | | Volume | Grain | 2 |
| | | | | Volume | Pore | 0 |
| | | | | Volume | ND[b] | 1 |
| | | | | Undetermined | | 2 |
| 1000 | 469 (47) | 590 | 14.05 | Surface | Grain | 15 |
| | | | | Surface | Pore | 2 |
| | | | | Surface | ND[b] | 0 |
| | | | | Volume | Grain | 0 |
| | | | | Volume | Pore[b] | 0 |
| | | | | Volume | ND[b] | 10 |
| 1371 | 520 (54) | 544 | 11.25 | Surface | Grain | 24 |
| | | | | Surface | Pore | 5 |
| | | | | Volume | Grain | 17 |
| | | | | Volume | Pore | 4 |

[a] Total specimen population, the numbers in parentheses indicate 1.0 standard deviation.
[b] Flaw nature was not determined (ND) for expediency.

TABLE II Censored Weibull parameters

| Temperature (°C) | Flaw[a] location | Number of specimens | Least squares fit | | Maximum likelihood | |
|---|---|---|---|---|---|---|
| | | | $\sigma_r$ (MPa) | $m_r$ | $\sigma_r$ (MPa) | Weibull modulus, $m_r$ |
| 25 | S | 26 | 694 | 18.36 | 694 | 18.65 |
| | V | 3 | 752[b] | 21.44 | 749 | 32.44 |
| | U | 2 | – | – | – | – |
| 1000 | S | 26 | 591 | 13.78 | 592 | 13.33 |
| | V | 1 | – | – | – | – |
| | U | 0 | – | – | – | – |
| 1371 | S | 29 | 565 | 10.12 | 574 | 8.86 |
| | V | 21 | 585 | 13.95 | 585 | 15.31 |
| | U | 0 | – | – | – | – |

[a] S: surface flaw; V: volume flaw; U: unknown origin.
[b] Estimated for three data points.

test temperature, and possibly a softening of the glassy phases surrounding grains of excessive length.

Weibull distributions (least squares) of bend strength for surface and volume flaws, determined using Equation 3, are illustrated in Fig. 5a and b, respectively. Both the maximum likelihood and least squares (LS) methods produced similar statistical parameters for censored data. Analysis of uncensored and censored data by the least squares method resulted in similar Weibull parameters, as shown in Table II for measurements at 1371 °C. As noted above, testing at 25 and 1000 °C resulted in too few volume failures for accurate comparison. Determination of the Weibull parameters for volume failure at low temperature may require either tensile testing or a large number of bend tests per condition.

## 3.3. Fracture toughness

Fracture toughness results are summarized in Table III. Room-temperature fracture toughness measured with the chevron-notch and the SEPB methods were comparable.

TABLE III Fracture toughness

| Test method | Temperature (°C) | Number of tests | $K_{IC}$ (MPa $m^{1/2}$) |
|---|---|---|---|
| Chevron notch | 25 | 5 | 7.9 ± 0.4 |
| | 800 | 5 | 7.1 ± 0.7 |
| | 1000 | 3 | 6.9 ± 0.3 |
| | 1200 | 4 | 6.0 ± 0.3 |
| | 1371 | 2 | 10.4 ± 0.5 |
| SEPB | 25 | 7 | 7.4 ± 0.5 |
| SENB | 1371 | 4 | 6.1 ± 0.4 |

Fracture toughness, measured with the chevron notch, decreased with temperature to 1200 °C. However, at 1371 °C the fracture toughness appeared to increase substantially. The corresponding load–displacement behaviour became severely non-linear with a much higher maximum load than exhibited by

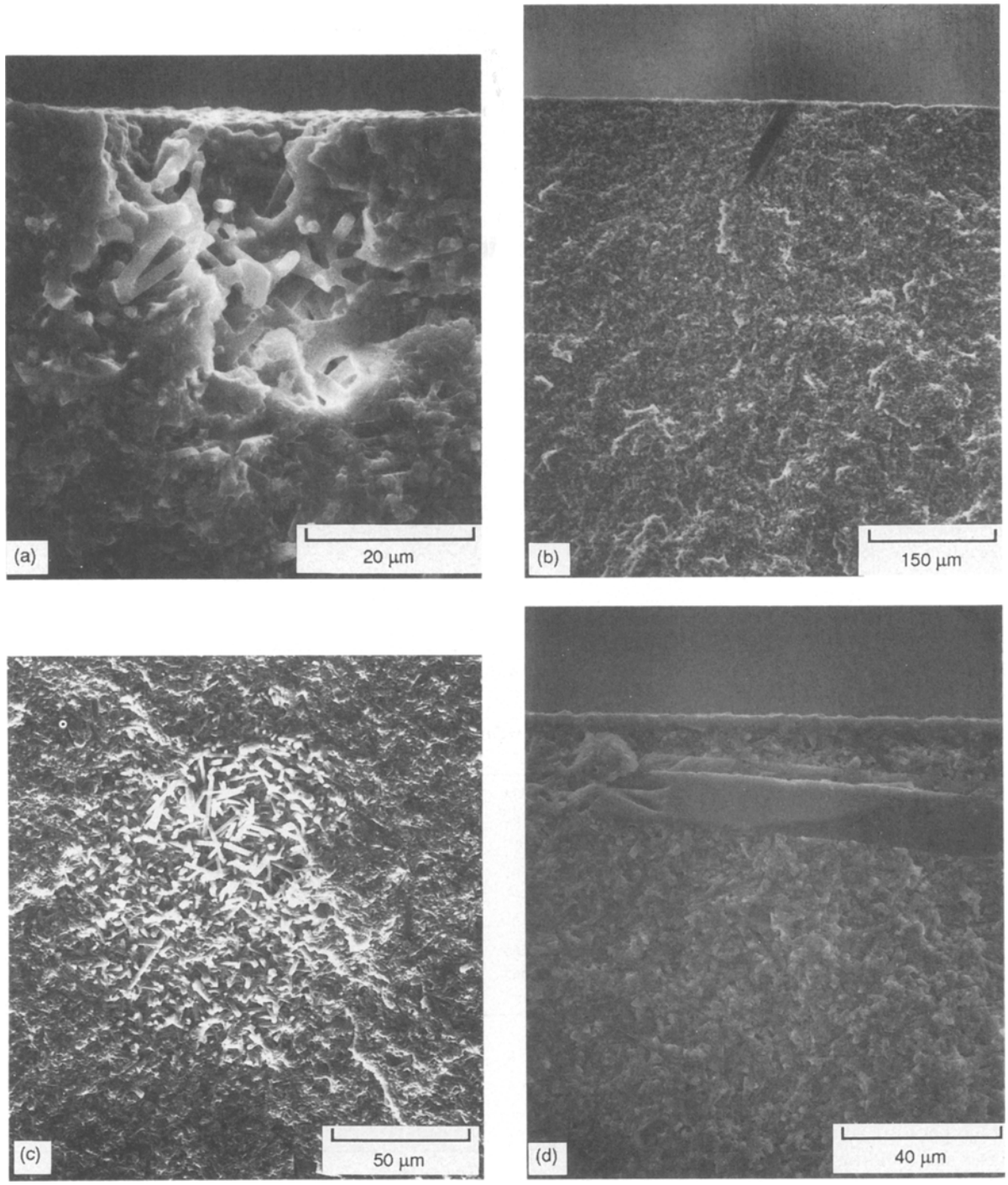


*Figure 3* Typical failure origins: (a) surface-connected pore; (b) large surface-connected grain; (c) volume pore; (d) large volume grain.

lower temperature tests. This maximum was followed by a large, residual load-bearing ability and incomplete failure of the specimen. Measurements with the SENB at 1371 °C were much lower and comparable to values measured with the chevron notch at 1200 °C. The SEPB specimen could not be used at elevated temperature because of precrack healing.

Typical room-temperature fracture topography of chevron-notched and SEPB specimens is illustrated in Fig. 6. Although some of the very large, elongated grains oriented normal to the crack plane were pulled out, a more typical occurrence was cleavage without deflection of the crack path. Grains oriented at low angles were partially separated from the matrix prior to cleavage. Small, well-bonded grains ($< 10\ \mu m$) failed in groups with grains extending out of the fracture surfaces.

Fracture surfaces of chevron-notched specimens tested at 1371 °C are shown in Fig. 7a and b. The cracked region, shown in Fig. 7a was heavily oxidized with some grains protruding out of the oxide layer. The crack-tip region where the crack stalled, shown in Fig. 7b, exhibited a relatively large concentration of exposed grains. Evidently, the crack stalled due to deformation and hinging of the ligament. The stalled crack was oxidized and the long, favourably oriented grains near the crack tip were pulled apart by viscous deformation of the grain boundaries. The deformation hinging thus resulted in the high maximum and residual loads displayed, and the high, apparent fracture

toughness. The grain pull-out was indicative of deformation instead of bridging, as high apparent toughness was also observed for fine grained silicon nitrides [11].

### 3.4. *R*-curve behaviour and its relation to Weibull modulus

Damage or flaw tolerance that results from an increasing resistance to stable crack propagation is a desirable property for structural ceramics. Krause [8] has shown that *R*-curve behaviour can be evaluated from indentation strength data, assuming that the fracture resistance, $K_r$, is related to the crack length, $c$, by a power-law relationship. The fracture resistance and the indentation strength, $\sigma_f$, relations are expressed by

$$K_r = kc^{\tau} \tag{4}$$

$$\sigma_f = \frac{k(3 + 2\tau)}{4\beta}\left[\frac{4P\Gamma}{k(1 - 2\tau)}\right]^{(2\tau - 1)/(2\tau + 3)} \tag{5}$$

where $k$ and $\tau$ are constants, $\Gamma$ and $\beta$ are the dimensionless quantities associated with the residual contact stress intensity and the crack geometry (defined in $K_I = \beta\sigma c^{1/2}$, where $K_I$ is the Mode I stress intensity factor and $\sigma$ is the applied stress) respectively, and $P$ is the indentation load. When $\tau = 0$, Equation 5 reduces to the case of no crack resistance toughening. Also, $K_r = K_{IC}$ for $\tau = 0$. The parameter $\tau$ was evaluated from the best-fit slope of the $\log \sigma_f$–$\log P$ data shown in Fig. 8. The constant, $k$, was evaluated from Equation 4 with the estimated $\tau$ and the toughness value obtained with the indentation strength method [12] for a crack size of $c = 102$ μm.

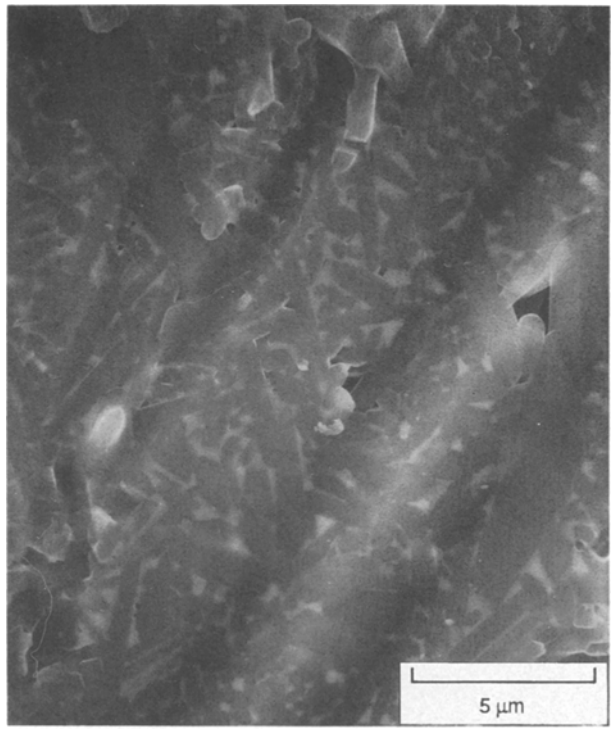


*Figure 4* Glassy region connected to a large grain that induced strength failure.

The *R*-curve estimation is presented in Fig. 9, where the fracture resistance curve is plotted as a function of the crack size based on Equation 4. For illustrative purposes, the fracture resistance curve for a silicon nitride (Norton 6% yttrium $Si_3N_4$ [11]) with an equiaxed microstructure (Fig. 10) is included [13]. It

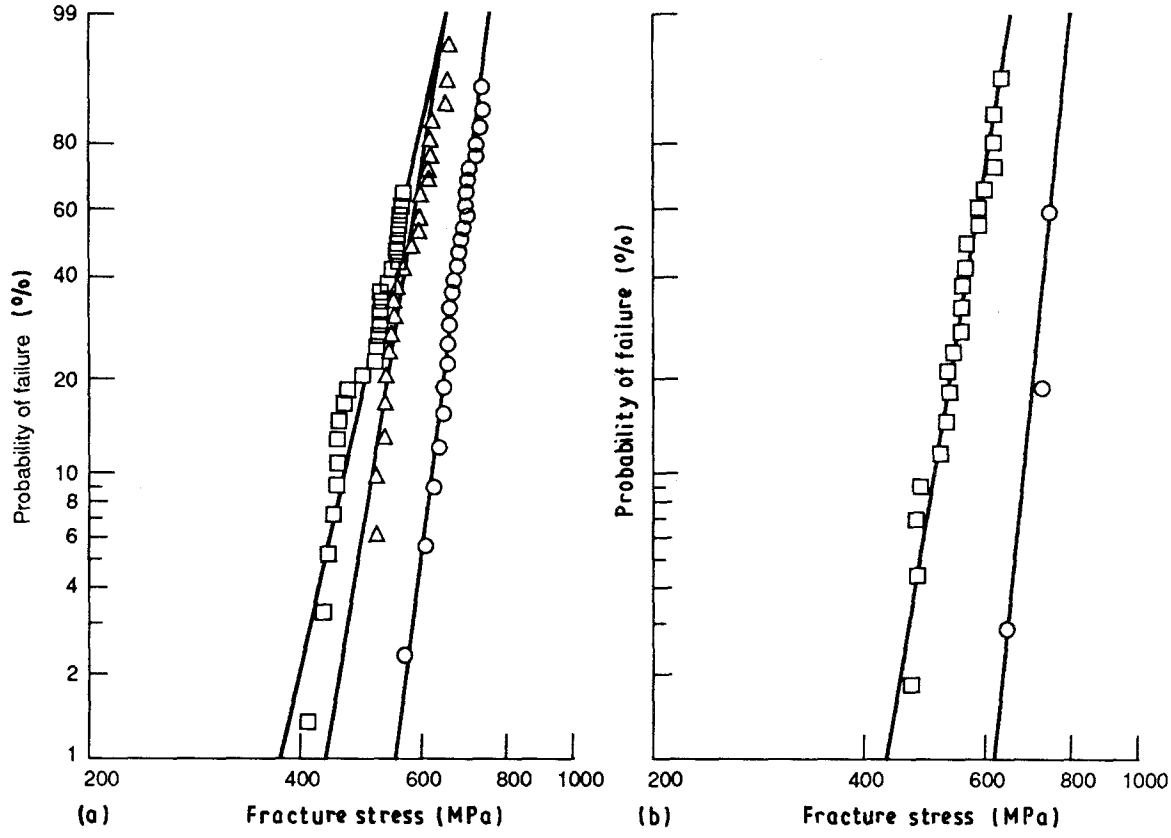


*Figure 5* Weibull distributions (least squares): (a) surface flaws; (b) volume flaws. (○) 25 °C, (△) 1000 °C, (□) 1371 °C.

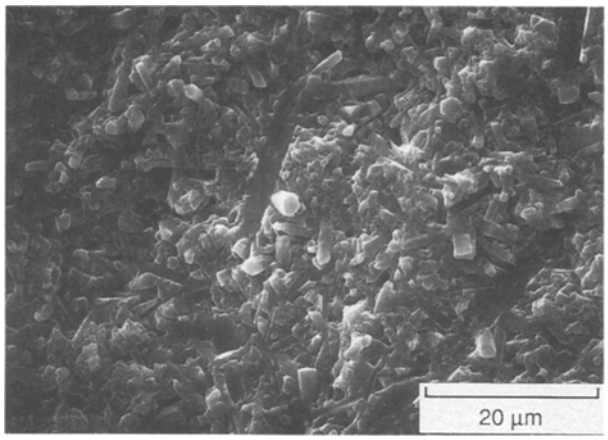


*Figure 6* Room-temperature fracture toughness topography.

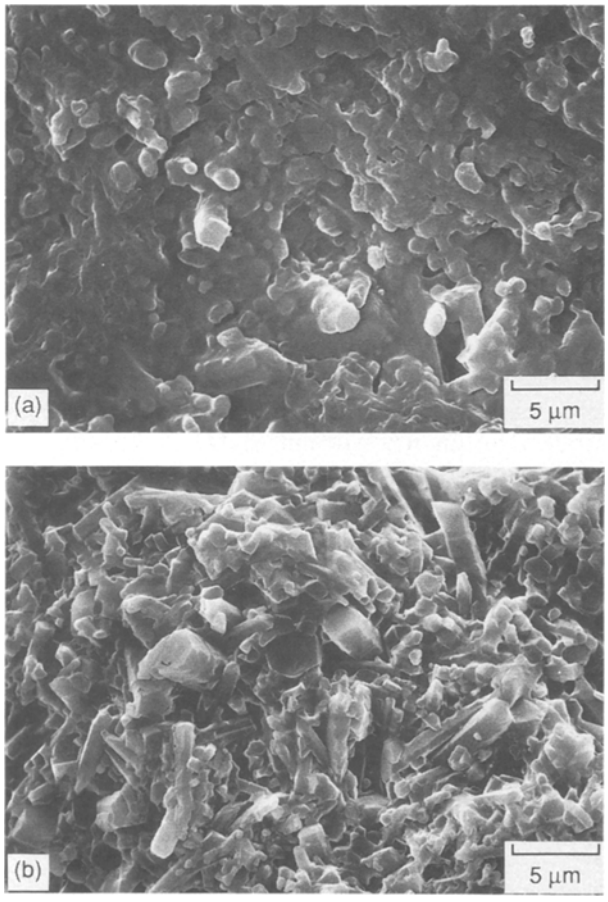


*Figure 7* Chevron-notch fracture topography for 1371 °C: (a) oxidized wake region; (b) crack tip.

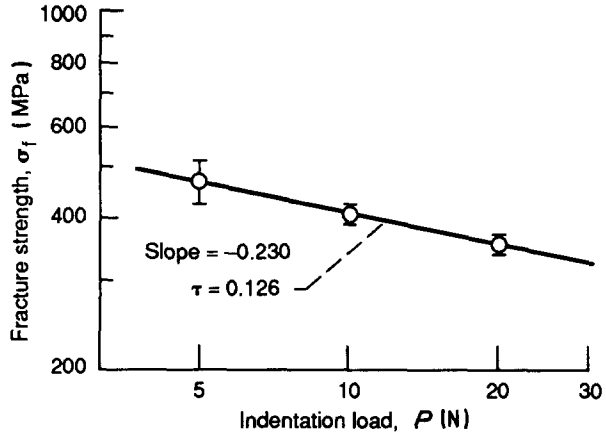


*Figure 8* Fracture strength as a function of indentation load for SN 251 $Si_3N_4$. Error bar indicates ± 1.0 standard deviation.

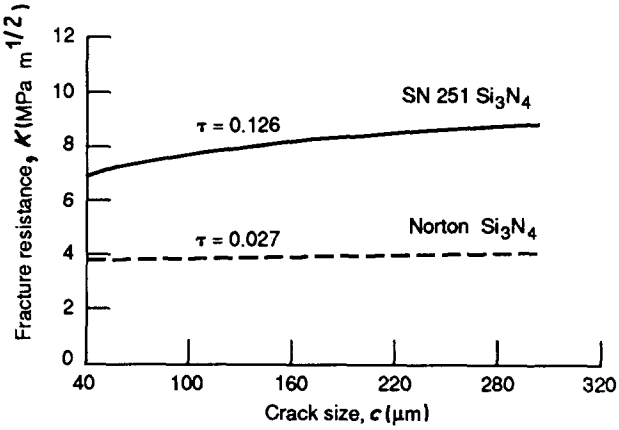


*Figure 9* Predicted fracture resistance curves for *in situ* toughened material with an equiaxed microstructure.

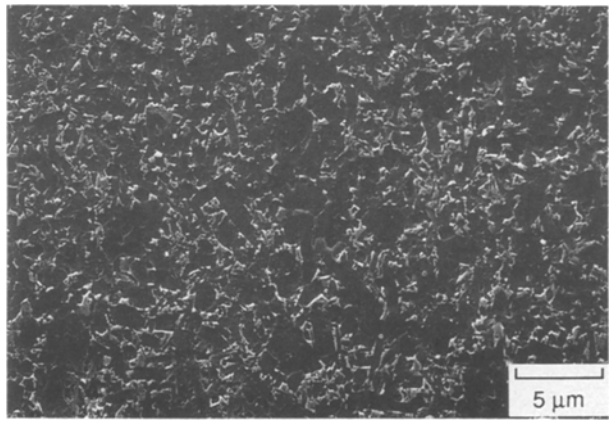


*Figure 10* Plasma-etched microstructure of a 6% yttrium silicon nitride with an equiaxed grain structure.

can be seen from Fig. 9 that the *in situ* toughened material exhibits strong *R*-curve behaviour with a toughening exponent of $\tau = 0.126$; whereas the material with an equiaxed microstructure exhibits a flat *R*-curve with a negligibly small exponent of $\tau = 0.027$, and a lower level of $K_r$. The elongated grain morphology not only increased the fracture toughness, but imparted crack growth resistance to silicon nitride. Similar observations of rising *R*-curve behaviour ($\tau = 0.1$–$0.22$) and improved fracture toughness were found in other *in situ* toughened silicon nitrides [14, 15].

Ceramics with a rising *R*-curve have been experimentally shown to exhibit a higher Weibull modulus as compared to ceramics with a flat *R*-curve. Kendall *et al.* [16], Cook and Clarke [17], and Shetty and Wang [18] made attempts to develop closed-form solutions for the modified Weibull parameters based on fracture mechanics principles and two-parameter Weibull statistics. A similar derivation of the modified Weibull parameters for the *R*-curve enhanced material, based on the procedure used by Shetty and Wang

[18], was made in this study and found to yield

$$m_r = \frac{m_0}{1 - 2\tau} \quad (6)$$

and

$$\sigma_r = \frac{kK_{IC}^{2\tau - 1}}{\sigma_0^{2\tau - 1}\beta^{2\tau}} \quad (7)$$

where $m_r$ and $\sigma_r$ are the Weibull modulus and characteristic strength of the material with *R*-curve behaviour (i.e. those measured in this study), respectively, and $m_0$ and $\sigma_0$ are the Weibull modulus and characteristic strength for a flat *R*-curve material with the same flaw distribution. The Weibull modulus, $m_r$, is the same as that derived by Kendall *et al.* [16] or Shetty and Wang [18]. However, the characteristic strength, $\sigma_r$, is different from that derived by Shetty and Wang [18] by a factor of $(\pi\beta^2/4)^{-\tau}$. Note that when $\tau = 0$ the parameters reduce to the $m_0$ and $\sigma_0$ for the flat *R*-curve material. It also should be noted that the characteristic strength, $\sigma_r$, in Equation 7 is not an explicit function of the given material, but rather depends on the functional form that is chosen to represent $K_{IC}$.

Equation 6 shows that the Weibull modulus increases with increasing toughening exponent. For the previously evaluated exponent, $\tau = 0.126$ and surface Weibull modulus of $m_r = 18.36$, the Weibull modulus of a flat *R*-curve material with the same surface flaw distribution is back-calculated as $m_0 = 14$, a value typical of the upper range for monolithic silicon nitrides. This indicates that *R*-curve behaviour increased the Weibull modulus by 34% as compared to a material with the same flaw distribution and a flat *R*-curve. The Weibull modulus for surface flaws, $m_r = 18.36$, was used in the above calculation because the value of $\tau$ was derived from surface indentations cracks, and the *R*-curve is not considered unique for crack extension from different flaws. However, if the value of $\tau$ associated with stable crack extension from volume flaws is known (the same growth pattern), then the analysis should be applicable to volume flaws as well as surface flaws.

Although several simplifying assumptions were made in the above analysis, this approach gives a quantitative insight to the increased Weibull modulus observed for materials with rising *R*-curves.

### 3.5. Crack trajectory

In an attempt to explain the greater room-temperature fracture toughness and crack-growth resistance of the *in situ* toughened material relative to the silicon nitride with an equiaxed microstructure, indentation cracks (Vickers indentation load = 98 N) were placed in polished sections of both materials. The crack trajectories, as observed by SEM, are shown in Fig. 11.

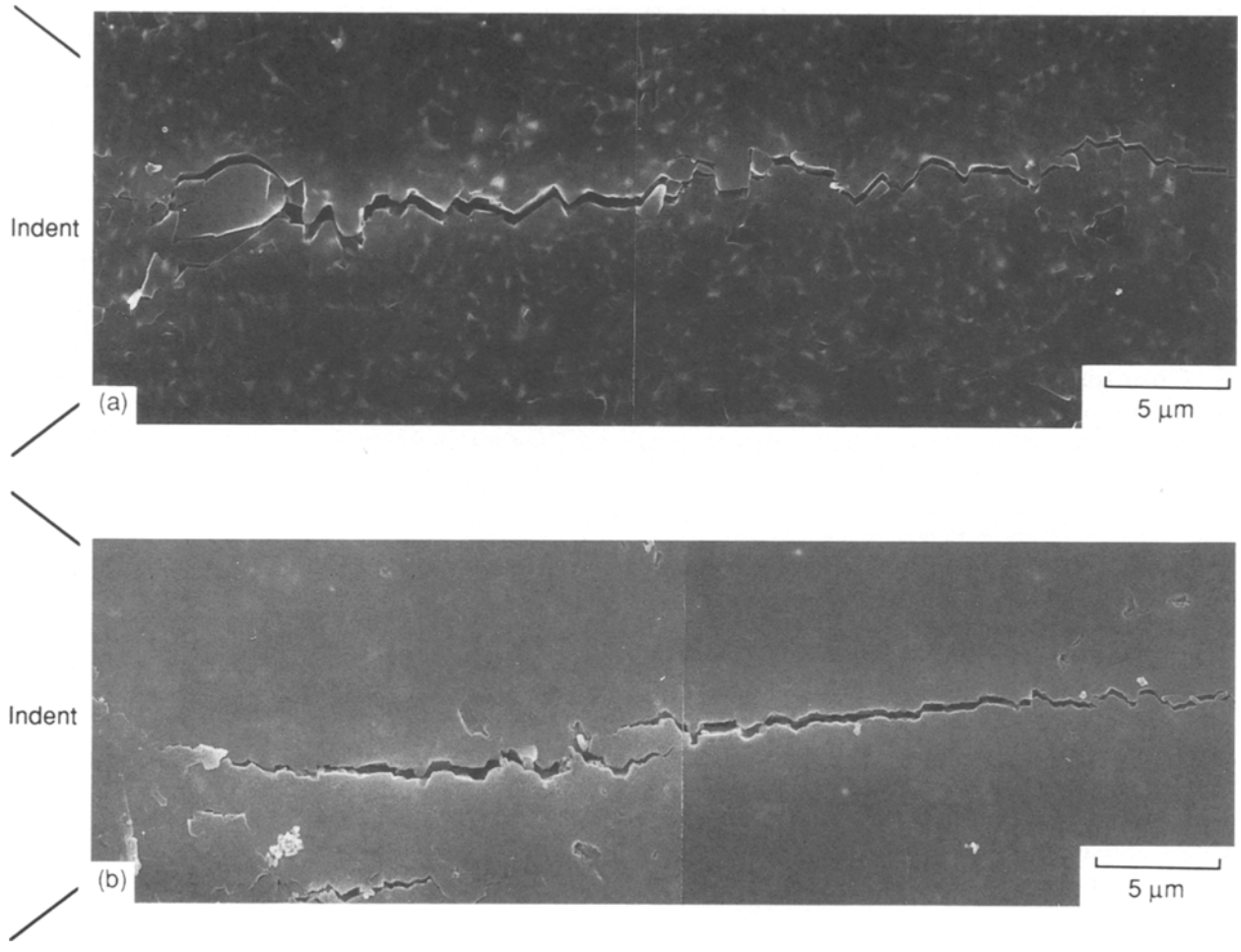


*Figure 11* Indentation crack trajectory for (a) *in situ* toughened silicon nitride and (b) silicon nitride with an equiaxed microstructure.

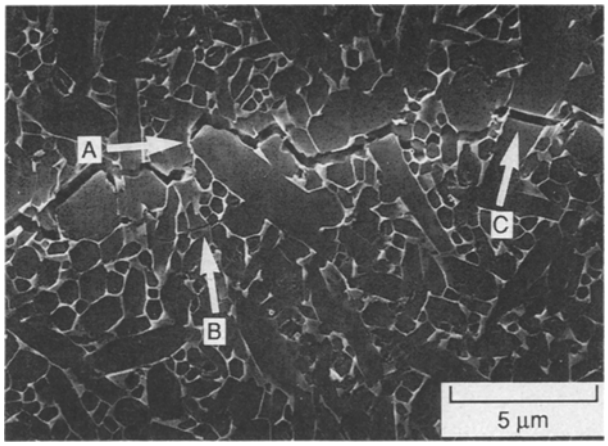


*Figure 12* Indentation crack trajectory for etched, *in situ* toughened silicon nitride.

The cracks traversed through the equiaxed microstructure with little deflection, but occasional bridging was apparent. In the *in situ* toughened material, however, the cracks followed a very tortuous path through the microstructure.

The crack path relative to the grain boundaries of the *in situ* toughened material is illustrated in Fig. 12. The crack passed through the boundaries of small grains as well as large grains oriented at low angles, resulting in crack deflection, interlocking, and bridging behaviour analogous with whisker pull-out. Note the wedging of the elongated grain relative to surrounding material (arrow A), and the resultant, secondary cracking (arrow B). Long grains oriented at large angles to the crack path were cleaved (arrow C). This crack interaction with the elongated grain structure may account for the improved fracture toughness and rising crack growth resistance of the *in situ* toughened material relative to the material with an equiaxed microstructure.

## 4. Conclusions

Silicon nitride with an elongated microstructure exhibited good elevated-temperature strength and a high Weibull modulus. Ultimate strength of the material was limited by excessively large, 30–100 μm grains, or 15–70 μm diameter pores. The excessively long grains were developed by a non-uniform distribution of sintering additives. The room-temperature failure origins were predominately surface-connected flaws. At 1371 °C the failure origins were frequently within the volume and the Weibull modulus decreased to approximately 11 from a room temperature value of 19. The increased incidence of volume failure and lower Weibull modulus were probably due to softening of the glassy secondary phases surrounding large grains, healing of surface flaws, and a possible loss of crack-growth resistance.

The SEPB and chevron-notch fracture toughness test methods resulted in similar measured values at room temperature. At 1371 °C, load rate and deformation effects unfavourably influenced fracture toughness measurements made with the chevron-notched flexure bar. Crack-growth resistance at room temperature ranged from 6.5–9 MPa within a 300 μm crack extension, resulting in a 34%, estimated enhancement of the Weibull modulus.

The improved fracture toughness, crack-growth resistance and Weibull modulus were attributed to the elongated grain structure, which resulted in significant crack deflection and bridging, as compared to that of a material with an equiaxed microstructure.

## Acknowledgement

The authors thank Oak Ridge National Laboratory for funding under contract DE-AI05-870R21749.

## References

1. J. A. SALEM, J. MANDERSCHEID, M. FREEDMAN and J. GYEKENYESI, *J. Gas Turbines Engng*, in press.
2. J. P. GYEKENYESI, *J. Engng Gas Turbine Power* **108** (1986) 540.
3. K. N. SIEBEIN and W. M. LOVINGTON, in "Microstructural Science", Vol. 16, "Metallography of Advance Materials", edited by H. J. Cialone (International Metallographic Society, Columbus, OH, 1988) p. 319.
4. "Young's Modulus, Shear Modulus, and Poisson's Ratio for Ceramic Whitewares by Resonance", ASTM Standard Test Method C848-88 (American Society for Testing and Materials, Philadelphia, PA, 1988).
5. T. NOSE and T. FUJII, *J. Amer. Ceram. Soc.* **71** (1988) 328.
6. D. MUNZ, R. T. BUBSEY and J. L. SHANNON Jr, *ibid.* **63** (1980) 300.
7. M. J. JENKINS, J. A. SALEM and S. G. SESHARDRI, *J. Compos. Mater.* **23** (1989) 77.
8. K. F. KRAUSE, *J. Amer. Ceram. Soc.* **71** (1988) 338.
9. K. JAKUS, J. E. RITTER Jr, T. SERVICE and D. SONDERMAN, *ibid.* **64** (1981) C-174.
10. S. A. SZATMARY, J. P. GYEKENYESI and N. N. NEMETH, NASA Technical Memorandum 103 247 (1990).
11. J. A. SALEM, NASA Technical Memorandum 102 423 (1990).
12. P. CHANTIKUL, G. R. ANSTIS, B. R. LAWN and D. B. MARSHALL, *J. Amer. Ceram. Soc.* **64** (1981) 539.
13. S. R. CHOI and J. SALEM, "Strength and Fracture Toughness Properties of Whisker Reinforced Silicon Nitride Matrix Composite and Monolithic Silicon Nitride", edited by Michael D. Sacks, Presented at the Symposium on Composites sponsored by American Ceramics Society, Orlando, FL, 12–15 November 1990 (The American Ceramic Society, Inc., Westerville, OH, 1991).
14. J. E. RITTER, S. R. CHOI, K. JAKUS, P. J. WHALEN and R. G. RATEICK, *J. Mater. Sci.* **26** (1991) 5543.
15. C. W. LI and Y. YAMANIS, *Ceram. Engng Sci. Proc.* **10** (1989) 632.
16. K. KENDALL, N. M. ASHFORD, S. R. TAN and J. D. BIRCHALL, *J. Mater. Res.* **1** (1986) 120.
17. R. F. COOK and D. R. CLARKE, *Acta Metall.* **36** (1988) 555.
18. D. K. SHETTY and J. S. WANG, *J. Amer. Ceram. Soc.* **72** (1988) 1158.

*Received 22 April*
*and accepted 5 August 1991*